Mozambique Channel Eddies in GCMs: A question of resolution and slippage

G.D. Quartly, B.A. de Cuevas, A.C. Coward

[Manuscript accepted by Ocean Modelling Dec 2012]

Abstract

Hydrographic observations in the 21st century have shown that the flow within the Mozambique Channel is best described by a series of large poleward-propagating anticyclonic eddies, rather than, as previously thought, a continuous intense western boundary current. The portrayal of this region in various runs of the NEMO 75-level model is found to vary between those two descriptions depending upon the resolution used and the implementation of the model's lateral boundary conditions. In a comparison of $^1/_4^\circ$ resolution runs, the change of these conditions from free-slip to no-slip leads to the mean southward flow moving further offshore, with greater variability in the zonal and meridional velocities as the flow organises itself into eddies, and a reduction in total transport. If a realization of a model is unable to get these aspects of the physical flow correct, then this will significantly reduce its ability to show a realistic biological signal or long-term response to climate change. Further south, beyond Durban, the application of no-slip conditions similarly causes the mean Agulhas Current to lie further offshore, making it much more able to simulate Natal Pulses.

Keywords — Indian Ocean: Mozambique Channel, NEMO, Spatial resolution, Boundary conditions, Stability, Natal Pulse (Current meandering)

1. Introduction

The Agulhas Current transports warm salty Indian Ocean water poleward, with a small proportion of that transitting into the South Atlantic in the form of Agulhas rings and near-coastal flow. Changes in this flow and the "leakage" into the South Atlantic can have major effects on the flows contributing to the Atlantic overturning circulation (Beal et al., 2011) and thus European climate. However, to fully understand and model the Greater Agulhas System, and the variability it produces in the heat and salt flux into the Atlantic requires a clear picture of the variability in the upstream sources, viz. the poleward flow within the Mozambique Channel and the westward input from south of Madagascar. The flow from the latter region is highly variable, with occasional direct westward jets, apparent retroflection and many eddies (see Quartly et al., 2006 for discussion), but in this paper we are going to concentrate on the flow within the Mozambique Channel for which two very different schemata exist.

Until recently there had been few major hydrographic campaigns within the Mozambique Channel, with the limited observations synthesised into a picture of a strong western boundary current (Fig. 1a), acting as a precursor to the Agulhas Current, though by the 1980s this view was being questioned with Saetre and Jorge da Silva (1984) reinterpreting the sparse cruise data as a broad semi-permanent gyral circulation occupying most of the width of the channel (dashed lines in Fig. 1a). However, a detailed survey of the western half of the channel (de Ruijter et al., 2002), and the insight from altimetry (Schouten et al., 2003), provided a more complex picture of anticyclonic eddies propagating down the coast (Fig. 1b). Such an interpretation was also bolstered by ocean colour imagery (Quartly and Srokosz, 2004), which confirmed that the majority of features show anticyclonic flow about them (Fig. 1c).

Sea surface height (SSH) data from satellite-borne radar altimeters give an indication of cyclones and anticyclones in this region. However, the interpretation of individual features must be performed with care, as the spatial separation of altimeter tracks is quite large (see Fig. 1d), necessitating 2-D interpolation to image the eddies. Also, the comparison of individual SSH tracks to a reference mean profile generates similar magnitude positive and negative anomalies, when reality may be simply a train of anticyclones interspersed by an absence of eddies. However, the map of SSH variability (Fig. 1d) does confirm that there are varying features on the west side of the Mozambique Channel, although these are less significant when the water depth is less than 1000m.

In fact, this is a region where numerical models had helped lead the way in interpretation of the flow regime, with a $^1/_3^\circ$ model by Biastoch and Krauss (1999) showing large anticyclonic eddies prior to the *in situ*

observations. However, more recently Lutjeharms et al. (2012) noted that a high-resolution (0.1˚) model of the region that normally shows anticyclonic eddies does provide fleeting glimpses of a coherent Mozambique Current. Possibly the full nature of the flow in the Mozambique Channel still has aspects yet to be fully revealed by numerical modelling. This paper examines output from a model, NEMO, run at different resolutions and with different lateral boundary conditions to show how sensitive the overall dynamic picture is to these choices.

2. Model Specification

The ocean model used in this study is the Nucleus for European Modelling of the Ocean (NEMO) in the ORCA1 (1˚), ORCA025 ($^1/_4$˚) and ORCA_R12 ($^1/_{12}$˚) configurations (Madec, 2008). The ORCA025 configuration is similar to the one used in Blaker et al. (2012). For all resolutions, the model has 75 vertical levels with layer thickness increasing from 1 m at the surface to more than 200 m at the bottom. The partial step option is applied which allows the bottom grid-cell thickness to vary at each location to give better topographic representation. The surface forcing consists of 6-hourly winds and daily fluxes for heat and freshwater from the DFS4.1 dataset (Brodeau et al., 2010). With a horizontal resolution of 0.25˚ ORCA025 is eddy-permitting, i.e. it can simulate ocean mesoscale eddies, but their dynamics is not resolved. Nevertheless, a horizontal resolution of $^1/_4$˚ has been shown to produce satisfactory eddy activity even if the eddy kinetic energy is lower than that suggested by satellite observations (e.g. Penduff et al., 2010). The 1˚ model is too coarse to resolve eddies, but is deemed appropriate for long climate runs, whereas the $^1/_{12}$˚ run can fully resolve eddies at low and mid-latitudes.

The standard lateral boundary formulation used for all the runs is a free-slip condition meaning that at the boundary there is no shear in the tangential flow (i.e. $\nabla \boldsymbol{v}.\boldsymbol{n}=0$, where $\boldsymbol{v}$ is the velocity vector and $\boldsymbol{n}$ is the unit normal to the boundary). The free-slip boundary condition is preferred for C-grid models (such as NEMO), where it is consistent with setting the relative vorticity to zero along the model boundary. NEMO provides the option of a no-slip lateral boundary condition, $\boldsymbol{v}\times\boldsymbol{n} = 0$, meaning that the tangential flow is zero at the boundary, but this can lead to erroneous boundary stress with stepped coastlines. However the magnitude of this stress can depend on the orientation of the coastline (Adcroft and Marshall, 1998; Haidvogel and Beckmann, 1999) and some applications may benefit when this stress substitutes for an unresolved process. To help investigate this possibility, a run with ORCA025 was also performed with the no-slip lateral boundary conditions. This was initialised from the state of the standard ORCA025 run at the start of 1997.

Output from all runs is available as 5-day averages, and is analysed to show how the simulated flow in the Mozambique Channel is affected by both resolution and choice of lateral boundary condition. Here we analyse the currents in layer 14, centred at 26.6 m, as this is typical of the near-surface flow. Correlation analysis (not shown) indicates that for most locations in this channel the meridional currents at any level in the top 100m have a correlation of at least 0.9 with those in the selected layer. This selected depth is also commensurate with that used for droguing surface drifters (typically 15m), and the depth of the mixed layer in this model (ranging from 35 to 45 m in the Mozambique Channel). Later in this paper, we also analyse the total transport integrated over the whole water column.

3. Mean state and variability

3.1. Near-surface velocities

Although the models are forced by high-frequency wind products, they cannot be expected to generate transient mesoscale oceanographic features at the same times and locations as found in hydrographic observations. Consequently the comparison here is of the models' ability to produce the expected features with the appropriate length scales and frequencies. The very different dynamic regimes, produced by the different runs of NEMO, are illustrated by the selected 5-day mean fields shown in Fig. 2.

As expected the 1˚ version of the model simply shows a slow and broad western boundary current (WBC) heading south (Fig. 2a). In contrast the standard $^1/_4$˚ run (commonly referred to as "eddy-permitting") shows a narrower and more intense WBC, but with a pronounced offshore northward current (Fig. 2b). A further increase in resolution to $^1/_{12}$˚ ("eddy-resolving") does indeed show a much more complex flow pattern

with two intense anticyclonic eddies hugging the western boundary, plus a number of other partial features (Fig. 2c). The $^1/_{12}^\circ$ run not only contains large anticyclones, but also has some smaller weaker features with cyclonic flow. What is striking about this sequence of images is that the standard $^1/_4^\circ$ resolution model fails to generate eddies in this region, whereas various models of comparable resolution have previously shown their existence to be common. For example a seminal paper by Biastoch and Krauss (1999) at $^1/_3^\circ$ resolution had clear large eddies, as did the $^1/_4^\circ$ version of OCCAM (Webb et al., 1998).

However, the extra run of NEMO at $^1/_4^\circ$ resolution produces poleward-travelling anticyclonic eddies (Fig. 2d) of roughly the size shown in observations. The only change from the model portrayed in Fig. 2b has been in the choice of lateral boundary conditions with the extra realization employing the "no-slip" condition. Simplistically such a frictional retardation may be expected to generate a cyclonic shear in the along coast flow; however its effect is to cause the flow to lie further offshore, where it is less topographically constrained, and thus enable it to break up into large anticyclonic eddies in response to the increasing (anticyclonic) relative vorticity gained by moving poleward.

To address whether the snapshots shown in Fig. 2 are representative, we calculated the mean flow and its variability in each model (Fig. 3). In the long-term mean there is a moderate (of order 0.4 m s^{-1}) poleward flow close to the coast, and all the model versions except the coarse resolution one show an apparent northward flow ~200 km further offshore. In terms of velocity variability, there is the expected order of magnitude increase in going from 1° to $^1/_{12}^\circ$ resolution, with the variability greatest near the region of strongest mean flow. Curiously the $^1/_{12}^\circ$ model has low variability at the narrows of the channel (16.5°S) where the eddies are believed to be produced (Harlander et al., 2009). Again the $^1/_4^\circ$ run with no-slip condition produces a variability map more similar to the $^1/_{12}^\circ$ free-slip run than the $^1/_4^\circ$ free-slip run. However, with the no-slip run the variability extends further north of the narrows, and is somewhat reduced in the southern third of the plot (Fig. 3d).

Comparative sections at 21°S are provided in Fig. 4. All the models evaluated here show a strong southward mean flow on the western side of the channel, and also a weak southward flow on the east. For the free-slip $^1/_4^\circ$ run, the offshore return current gives a northward mean flow at 37°-37.5°E, whereas the models that do produce eddies ($^1/_{12}^\circ$ free-slip and $^1/_4^\circ$ no-slip) have their northward flow at 38°-39°E. However the mean southward flow in the no-slip run is weaker and further offshore than in the free-slip cases.

Figure 5 shows an examination of the dynamic height field (in effect a depth-integrated measure, in contrast to the individual layers shown in Figs. 2 and 3). Model output was considered for the years 1997 to 2001 and a simple sinusoid used to fit and remove the seasonal cycle at each location. White contour lines show the mean: the $^1/_4^\circ$ free-slip run (Fig. 5b) has as many closely-spaced contours along the west of the channel as the $^1/_{12}^\circ$ run, whilst the $^1/_4^\circ$ no-slip run (Fig. 5d) has fewer contours there, but more to the south of Madagascar, implying that these two Agulhas source regions contribute different proportions in the no-slip run to the other runs. Colours indicate the variability in dynamic height, with both $1^\circ$and $^1/_4^\circ$ free-slip runs having very little variability in this region (consistent with near-constant flows and no eddies). The $^1/_{12}^\circ$ free-slip and $^1/_4^\circ$ no-slip runs do have significant variability (0.1 to 0.2 m) on the western side of the channel, principally along the locations where the mean field is highest. The overall magnitude of variability is not as high as shown in altimetry (Fig. 1d), which does also include measurement noise, and the regions of variability differ between these two model runs in the same manner as for near-surface current variability (Fig. 3).

3.2. Vorticity analysis and instability

To help understand the differences in this region, we compute the relative vorticity averaged over the 25-200 m depth range (though essentially the same results are found if we focus on a single layer). The broad flow of the 1° model contains little vorticity, whereas a snapshot of the $^1/_4^\circ$ free-slip run has a continuous band of positive relative vorticity between its Mozambique Current and the offshore return, with weaker strips of negative vorticity on either side. Individual snapshots vary little, so the same pattern is present in the mean (Fig. 6a). As can be inferred from Fig. 2c,d, snapshots of the $^1/_{12}^\circ$ free-slip and $^1/_4^\circ$ no-slip have large discrete blobs of positive vorticity surrounded by haloes of negative relative vorticity. The $^1/_{12}^\circ$ model also has some small cyclones. Although in the mean both models have a western band of positive vorticity (Fig. 6b,c) this band is weaker and broader than for the $^1/_4^\circ$ free-slip case. The non-slip realization

also has this band further offshore, with consequently the transition line between negative and positive relative vorticity lying in deeper water where it is more susceptible to instability.

Cronin and Watts (1996) introduce a term for barotropic instability (BTI), which is commonly interpreted as the rate of barotropic conversion of kinetic energy from the mean to the eddy field. Following Biastoch and Krauss (1999), we integrate this down to 1100m viz:

$$BTI = \int - \left(\overline{u'u'} \frac{\partial \bar{u}}{\partial x} + \overline{u'v'} \left(\frac{\partial \bar{u}}{\partial y} + \frac{\partial \bar{v}}{\partial x} \right) + \overline{v'v'} \frac{\partial \bar{v}}{\partial y} \right) dz \qquad (1)$$

where u, v are components of the velocity in the horizontal x, y directions respectively, the overbar indicates a time-average and prime the deviation from the mean. Not surprisingly, the magnitude of this term is small for the $^1/_4^\circ$ free-slip run (Fig. 6d), but bands of similar magnitude are found for the $^1/_4^\circ$ no-slip and $^1/_{12}^\circ$ free-slip runs (Figs. 6e,f). The interesting difference between these two is that the $^1/_4^\circ$ no-slip run has the peak in this barotropic instability term just to the north of the narrows in the channel, whereas for the $^1/_{12}^\circ$ run the production of eddy kinetic energy occurs south of 17˚S and is at its greatest at the southern end of the Mozambique Channel.

3.3. Depth structure and bottom interaction

A further perspective on the mean flow is provided in Fig. 7, which gives vertical sections of the average meridional current at 16.5˚S and at 21˚S. A non-linear colour scheme is used to enhance the clarity of changes near zero. In the mean, significant southward flow (>0.05 m s^{-1}) is confined to the western 150 km and the top 1500 m. Similar to the near-surface manifestations of the mean current (Fig. 3), the deep core of the flow in the $^1/_4^\circ$ no-slip run (Figs. 7b,e) lies further offshore than for either of the other runs. The high-resolution run shows an apparent connection of the northern offshore flow at the surface to the core of the Mozambique Undercurrent on the shelf edge at 1500-2500 m (Figs. 7c,f); whilst both the $^1/_4^\circ$ realizations have a northward undercurrent distinct from the surface return. Figure 2a of van der Werf et al. (2010) shows the mean for 4.2 years of mooring data at 16.5˚S, with southward mean flow occurring west of 41.5˚E down to 1500m, with the speed in most of the top 1000m being more than 0.05 m s^{-1}. This most closely matches the simulation in Fig. 7b, albeit with the mean southward flow close to the western shelf edge. From analysis of ALACE floats, Chapman et al. (2003) suggest that at this latitude, the flow at ~800 m depth will be weakly to the south in the eastern half of the section too; this is not shown by any of the models other than the 1˚ realization (not shown). Long-term observational means do not exist at other latitudes in the Mozambique Channel, but occasional hydrographic sections (e.g. de Ruijter et al., 2002) have also shown evidence of a Mozambique Undercurrent at 1500-2500 m unattached to any equatorward flow at the surface.

Following the example of Penduff et al. (2007), we calculate topostrophy i.e. the degree to which the temporal mean flow aligns with depth contours. This is because fluctuating currents caused by eddies will interact with the bathymetric gradient to generate a mean current in the propagation direction of topographic Rossby waves (Merryfield and Scott, 2007). This is calculated for all separate combinations of bottom depth and water layer depth, using the global output of the model to allow enough records for each combination to provide a statistically meaningful average. Using the formulation of Penduff et al. (2007), a correlation value of +1 implies that the current vectors for those conditions are always perfectly aligned with bathymetric contours, and directed in the direction of the topographic Rossby waves (here southward along the African coast), -1 that the flow is aligned in the opposite direction, and zero implies no correlation. Care is needed in interpreting absolute values as a number of other factors e.g. wind-driven surface circulation may produce cyclonic flow within oceanic basins; what is of greater import is how topostrophy varies between different model realizations with the same forcing. Our results confirm that the bottom currents are most strongly influenced by bathymetry, and that this steering is more pronounced at higher resolution (Figs. 8a-c). The implementation of no-slip boundary conditions, does, in general, reduce this effect (Fig. 8d); however the effect in surface waters is only a reduction from ~0.4 to ~0.2, and for water depths over 3000m the effect is negligible.

4. Temporal variability

Concentrating on the $^1/_4^\circ$ runs, we find that the Hovmöller diagrams at 21˚S (Fig. 9) emphasise the differences. For the standard run, the flow between 35.5˚ and 36.5˚E is permanently southward, with the flow near 37.5˚E being at least 0.1 ms^{-1} northward for over half the time, but with very short-term pulsing. In contrast, the run with no-slip conditions shows approximately 5-6 events a year which exhibit a strong poleward flow at 36˚E and opposing northward flow at 38˚E. These events are consistent with an eddy moving southwest through the section over a period of around 30 days. [Note that the no-slip run commenced at the start of 1997 from the model state of the free-slip run; the absence of eddy signals in the first 6 months is consistent with the time needed for such a model to adapt to different numerics (Penduff et al., 2007).] A Hovmöller analysis along a line parallel to the coast (not shown) indicates these features to be coherent from ~14˚S to 27˚S. The flow at 1046m (layer 47, not shown) has similar (but weaker) patterns to those illustrated in Fig. 9b; that the eddies should be moving slightly westward as they migrate through 21˚S is consistent with the isobaths shown in Fig. 1b.

Equivalent analysis for the $^1/_{12}^\circ$ run (Fig. 9c) shows typically 5 events per year, with signals propagating from the eastern half of the channel, but without the regularity seen in the $^1/_4^\circ$ no-slip realization. The high-resolution run has markedly more current variability in the eastern half of the section (Fig. 3c), but these signals may not be solely eddies but also alternating currents associated with Rossby waves in the channel. Figure 4b shows that the variability in the currents for all 4 models, with similar profiles for the meridional and zonal currents, with the peaks just offshore of the strong southward flow and then reducing gradually eastwards. For the free-slip models the $^1/_4^\circ$ run has ~3 times as much variability as the 1˚ run, and the $^1/_{12}^\circ$ run is a factor of 3 more variable than the $^1/_4^\circ$ one. Application of no-slip conditions to the 0.25˚ run produces similar levels of variability to the $^1/_{12}^\circ$ free-slip run.

Finally we examine the spectra of the variability at 21˚S. For this we consider the meridional flow from the 10-yr period 1998-2007. First we take the time series of 26.6m meridional currents at the location of greatest variability (see Fig. 4b). These time series of 730 points are analysed using Welch's periodogram method to give a robust estimate of the spectra. (This is achieved by averaging the results of nine overlapping 2-yr segments.) The spectra shown in Fig. 10a indicate the frequencies corresponding to the mesoscale variability. The $^1/_4^\circ$ run with no-slip boundary conditions has a peak in variability in the band 5-7 events per year roughly matching in location and amplitude that shown by the free-slip $^1/_{12}^\circ$ run. However the variance present in that frequency band for the standard $^1/_4^\circ$ run is a factor of ten less with no discernible peak. Altimetric analysis by Schouten et al. (2003) finds approximately 4 anticyclonic eddies per year at the southern end of the channel, but that variability at the northern end of the channel has spectral peaks at 5-7 events per year.

A very different picture emerges when we consider the total southward transport through the Mozambique Channel at 21˚S (Fig. 10b). For these modelled series there is a clear annual component (see Table 1), although such a strong seasonality is less obvious in observations (van der Werf, 2010). Although the 1˚ run does not have a significant peak in the frequency band shown, all the others do, with the spectra from both $^1/_4^\circ$ runs being similar to that for $^1/_{12}^\circ$, although slightly weaker.

5. Summary and Discussion

5.1 Spatial resolution

Numerical models provide an important tool for understanding aspects of the current oceanic circulation, and for predicting the changes associated with different forcing scenarios. If using a well-designed model with appropriate parameterizations of the physics, it is generally expected that improving the resolution will lead to greater fidelity in the portrayal of the ocean currents and eddies. Focussing on the flow within the Mozambique Channel, we note a change in the dynamics of the standard (free-slip) run of NEMO from a broad sluggish western boundary current at 1˚ resolution (Fig. 2a) to a more intense WBC at $^1/_4^\circ$ (Fig. 2b) and finally a chaotic conglomerate of eddies at $^1/_{12}^\circ$ (Fig. 2c). This change in the flow regime leads to much greater variability (Fig. 3) in keeping with the picture from altimetry (Fig. 1d). There are also marked changes in terms of the deep flow, specifically the northward-flowing Mozambique Undercurrent. The 1˚ resolution run has no northward flow in the mean at the narrows of the channel (not shown), whilst the $^1/_4^\circ$ run has a well-defined undercurrent near 1500 m (Fig. 7a) similar to real world observations.

However, the increase in resolution to $^1/_{12}^\circ$ leads to a much stronger Mozambique Undercurrent (Figs. 7c,f) than found in reality.

However, full eddy-resolving high-resolution is not always practicable, because of the increased loads on computer memory, processing time and storage. The incorporation of complex multi-component biology and nutrients into a model makes a significant impact on the processing and storage required. Consequently global biological models are rarely run at the same resolution as state-of-the art ocean circulation models. This is important because eddies and episodic offshore currents affect the transport of sediment, nutrients and larvae out into the channel. Only runs containing eddies can possibly replicate the patchiness in nutrient distribution likely to explain the satellite observations of chlorophyll (Quartly and Srokosz, 2004) and the abundance of ultraplankton species (Zubkov and Quartly, 2003). This supply of somatic reserves into mid-channel in turn affects the ecological system at higher trophic levels e.g. in the seasonal breeding of terns (Jaquemet et al., 2007). Similarly, century-long simulations to explore climate change associated with future warming scenarios also produce an unacceptable load on the highest-resolution models. This is due to the need to consider different environmental forcing or from the desire to perform multiple realizations to enable statistical measures of uncertainty from the ensemble. Finally there are a number of operational applications (search and rescue, pollution monitoring etc.) for which, even with regional models of limited domain, local agencies lack the computing resources to run models at the highest resolution. Therefore, it is interesting to look at how subtle changes in model numerics affect the representation of this region.

5.2 Boundary conditions

The $^1/_4^\circ$ no-slip run was initialised at the start of 1997 from the model state of the $^1/_4^\circ$ free-slip realization. It led to a profound change in the flow regime, with large eddies apparent throughout the western half of the Mozambique Channel, with the flow transition complete within 6 months (Fig. 9b). These changes not only affect the instantaneous view, but also the characteristics of the mean and variance of the currents in the channel. Backeberg et al (2009) used snapshots of the vorticity field to demonstrate the pronounced difference between two models of the Agulhas Current. Although not shown here the very different vorticity fields for the period shown in Fig. 2 are easily imagined. In this paper we have focussed on the 5-year mean to demonstrate that the applied lateral friction causes the mean flow to lie further offshore (Fig. 3), with the inshore transition to negative vorticity also being in deep waters (Fig. 6b). This increases the potential for instability, allowing the flow to break up into anticyclonic eddies. Consequently even the time-average flow is less directly steered by the prevailing depth contours (Fig. 8). This results in a broader but weaker mean current (Fig. 4a), with greater variability in both the meridional and zonal components (Fig. 4b), which more closely match the high-resolution free-slip run. However, the no-slip run produces variability further north than occurs in either the $^1/_{12}^\circ$ free-slip run or altimetry raising the question as to whether it is allowing the correct physical processes to be modelled.

The change to no-slip conditions also affects the flow at depth, with the mean section for the $^1/_4^\circ$ no-slip run at 16.5˚S (Fig. 9) more closely matching both the sectional profile of mooring observations and reducing the total transport from ~25 Sv to ~17 Sv (Table 1). Although it might seem surprising that models varying in resolution from 1° to $^1/_{12}^\circ$ concur on the total flow, this arises because the flow is set by the Indonesian Throughflow plus the large-scale momentum balance integrated around a closed contour (Godfrey, 1989). Matano et al. (2008) showed that because of bathymetry blocking barotropic signals, only the western part of the South Indian Ocean contributed to the seasonal variation, which van der Werf et al. (2010) calculated to be a 4.5 Sv amplitude signal peaking in August. Consequently most models with realistic wind forcing (whether high temporal resolution or monthly climatology) have a similar response of amplitude 5 Sv with the peak flow delayed by a month due to the time needed for the signal to propagate via the South Equatorial Current (SEC) to the Mozambique Channel.

A decreased total transport for no-slip conditions is a feature endemic to many other models, with reductions noted, for example, for the Gulf Stream and Kuroshio Current (Haidvogel et al., 1992; Verron and Blayo, 1996). In the case of the Mozambique Channel it can be conjectured that the existence of a viscous boundary layer effectively reduces the width of the channel by ~25 km on each side. For the other currents mentioned the reduction is seen as a problem, but here the total transport for the no-slip run appears the closest to reality. Individual one-time sections show a wide range of values (e.g. Di Marco et al., 2002), but a median of their cited hydrographic sections (at various latitudes) is ~14 Sv, similar to that from the moorings at 16.5˚S (de Ruijter et al., 2002; van der Werf et al., 2010). The latter authors note that there is

significant high-frequency variability in the time series, with a spectral peak around 5-7 events per year. Spectral analysis of the time series from these models shows that whilst for the $^1/_4^\circ$ free-slip run such a peak is absent in the near-surface circulation (Fig. 10a), it is present in the total integrated transport (Fig. 10b). In this case it is manifest as pulses of a near-continuous western boundary current but for other runs it is associated with eddies forming/squeezing through the narrows. This lends support to the assertion by Backeberg and Reason (2010) that such high-frequency variations are at least partially controlled by spurts of extra vorticity within the SEC rather than being solely set by dynamics internal to the Mozambique Channel.

Reduced gravity quasigeostrophic simulations of the Florida Current by Mariano et al. (2003) illustrate the impact of the change to no-slip conditions for a simple case without bathymetry — again the result is a switch from a nearly uniform WBC to a set of, admittedly regular, eddies. Speich et al. (1996) found no-slip conditions essential for modelling of the Alboran Gyre: application of free-slip conditions in this narrow *zonal* channel caused the distending of the gyral flow through interactions with mirror image flows within the boundary. Over the past 15 years there have been many different eddy-permitting regional or global models, and with hindsight the impact of boundary conditions can be seen in their different results. AGAPE (Biastoch and Krauss, 1999) and OCCAM025 (Quartly et al., 2005) both showed eddies or eddy-related variability in the Mozambique Channel. Both of these were B-grid models for which no-slip conditions are preferred by the modelling community. Of the many models considered by van der Werf et al. (2010), most of the eddy-permitting runs were of B-grid models and the vertical sections across 16.5˚S show these to have a mean "Mozambique Current" core slightly displaced from the western shelf. They also note that ORCAO25 does not produce any eddies, and that the mean modelled transport ranges from 11.3 Sv for OCCAM025 to 23.6 Sv for ORCA025. Our detailed investigation using multiple realizations of a single model with identical forcing indicates that much of their observed difference is likely to be due to the choice of slippage.

Thus for this particular case study, there appear to be many benefits of employing no-slip conditions — production of eddies, offshore transport of nutrients, larvae etc., improved mean vertical structure at choke point, and a reduced mean transport closer in line with observations. However free-slip has been more popular in the modelling community, especially for models formulated on the Arakawa C-grid, which is the more appropriate choice to conserve vorticity. The application of free-slip has generally given improved performance in terms of separation point for the Gulf Stream (Penduff et al., 2007; Verron and Blayo, 1996), larger total transport in WBCs (Penduff et al., 2007; Fransner, 2012) and greater variability in the trajectories of Agulhas rings (Penduff et al., 2007). There is an expectation that at sufficiently high-resolution and reduced levels of viscosity, the choice of free-slip or no-slip will have little impact on modelled ocean circulation (Adcroft and Marshall, 1998). However, recent work on the currents around the southern tip of Greenland in $^1/_{12}^\circ$ models has also shown no-slip conditions to have advantages (Bourdallé-Badie, pers. comm., 2011). This is at a latitude of 60˚N where the Rossby radius of deformation is much smaller, closer to the grid size. A recent paper by Deremble et al (2010) has looked at different means of implementing no-slip boundary conditions such that the benefits associated with free-slip runs are also achieved, but such ideas have yet to be independently evaluated.

5.3 Further example

In our study of the Mozambique Channel, one of the marked changes in portrayal upon switching lateral boundary conditions was the clear increase in eddy kinetic energy (EKE). However, an assessment of the global changes in EKE did not give a clear picture of where no-slip conditions would always make a pronounced difference. There are places of enhanced or diminished EKE associated with several of the WBCs, but in many cases this relates to a different location of their extensions and hence of where their variability occurs.

Figure 11 provides an illustrative example of how a change of lateral boundary conditions does affect current variability in another region. The location off the southeast edge of South Africa is just a little downstream from the Mozambique Channel, but has a very different flow regime, with all models showing a well-defined deep fast-flowing Agulhas Current, with eddies (originally from the Mozambique Channel or from south of Madagascar) occasionally present on the seaward side. Temperature is shown at ~100m depth, as that is free from effects of short-term atmospheric interaction.

The display of the two means (Figs. 11a,b) show the broad Agulhas Current, ~2˚C warmer than the surrounding waters, but with the core for the no-slip run lying further offshore. Large warm core

anticyclonic eddies impinge on the edge of the current in both runs. For the no-slip realization these eddies may lead to enhanced Agulhas flow, current instability and the development of a large offshore meander termed a Natal Pulse. The series of snapshots in Fig. 11c-e and Fig. 11f-h indicate that these solitary meanders propagate southwestwards at between 15 and 25 km day^{-1}, in keeping with the speeds noted by de Ruijter et al. (1999). Such features occur rarely, if at all, in the free-slip realization.

This is an extension of the idea that no-slip conditions push the current further offshore, making it more able to respond to instabilities — in this case not the whole flow breaking up into eddies, but permitting a realistic portrayal of solitary meanders. Whilst this is an aside from the main focus on the Mozambique Channel, it is clearly of great importance in terms of sensitivities within the linked global circulation. Natal Pulses may play a significant role in the early retroflection of the Agulhas Current (Lutjeharms and van Ballegooyen, 1988), a phenomenon that precludes any Indian Ocean water from reaching the Atlantic for months at a time (Fig. 5 of Srokosz, 2003). It would seem essential that any global ocean model being run for climate-scale investigations should be configured so that Natal Pulses are within the scope of its simulations.

For climate studies, the ultimate goal for the Agulhas region would be the correct numerical portrayal of the leakage of warm salty water from the Indian Ocean into the Atlantic, which is the sum of not only the pronounced rings shed by the Agulhas Retroflection, but also the coastal flows. Differences can be seen here between the $^1/_4^\circ$ runs with no-slip or free-slip conditions. For example, the no-slip run appears to have a more regular trajectory for Agulhas rings (cf. Penduff et al., 2007) and greater variability further downstream within the Agulhas Return Current. However, a diagnosis of whether these are due to local or upstream effects, and the implications for total heat and salt transport between the Indian and Atlantic Oceans is beyond our intentions for this paper.

6. Conclusions and recommendations

Chassignet and Marshall (1998) note that a great many factors (resolution, grid orientation, partial steps, momentum advection scheme, diffusivity operator) can affect a single aspect of a model — in their case, western boundary current separation. This investigation confirms the consensus that increasing the resolution of numerical models will generally improve the realism of their representation of currents, in this particular case including a switch from a strong continuous western boundary current to an eddy-rich regime. Intriguingly, for this particular location, an alternative formulation of the lateral boundary conditions from free-slip to no-slip achieves a very similar result to a factor of three improvement in resolution. This change in boundary conditions also leads to a reduction in transport, which in this particular case is beneficial. However, a number of other authors have previously noted a degradation in performance associated with no-slip. Given that very high-resolution runs are not practicable for all applications, further work on the specification of boundary conditions, including partial slip options, should be considered. An issue raised by Adcroft and Marshall (1998) is the complexity of the boundary conditions when the coastline runs obliquely across the model grid, producing a zigzag edge. Regional models can overcome this by having a grid with one of its horizontal axes running parallel to the coastline or shelf break e.g. SAfE (Penven et al., 2006).

The different dynamical behaviour associated with free-slip and no-slip runs can, with hindsight, be noted in many previous papers e.g. the eddies in OCCAM025 (Quartly et al., 2005) and the changes in offshore location of the current and the differences in transport (van der Werf et al., 2010). However, the elucidation of such an effect has been time-consuming as the regionally varying implications of the choice of boundary conditions is not widely recognised, and the details rarely reported. We recommend that authors using model output in their own oceanographic analyses are encouraged to include the words "free-slip" or "no-slip" in their brief description of the model.

Acknowledgements

This work was supported under NERC's "National Capability" programme. 'The ORCA025 simulations were undertaken on the UK National HPC service (HECToR) funded by the Natural Environmental Research Council. The ocean colour data were obtained from NASA/GSFC Ocean Color web portal, and the gridded altimetry data were the "update" product provided by CLS/Aviso. We are

grateful to Joel Hirschi, Gurvan Madec, Meric Srokosz and George Nurser for reading early drafts, even if their suggestions did give the authors further work to do. Thanks also to Issufo Halo for discussion on energy transfers in numerical models.

References

Adcroft, A., Marshall, D., 1998. How slippery are piecewise-constant coastlines in numerical ocean models?. *Tellus* 50A, 95-108.

Backeberg, B.C., Bertino, L., Johannessen, J.A., 2009. Evaluating two numerical advection schemes in HYCOM for eddy-resolving modelling of the Agulhas Current. *Ocean Sci*., 5, 173-190.

Backeberg, B.C., Reason, C.J.C., 2010. A connection between the South Equatorial Current north of Madagascar and Mozambique Channel Eddies. *Geophys. Res. Lett*. 37, art. no. L04604, doi:10.1029/2009GL041950

Beal, L.M., de Ruijter, W.P.M., Biastoch, A., Zahn, R., SCOR/WCRP/IAPSO Working Group 136, On the role of the Agulhas system in ocean circulation and climate, Nature, 472, 429-436. doi:10.1038/nature09983

Biastoch, A., Krauss, W., 1999. The role of mesoscale eddies in the source regions of the Agulhas Current. *J. Phys. Oceanogr*, 29, 2303-2317.

Blaker, A.T., Hirschi, J.J-M., Sinha, B., de Cuevas, B., Alderson, S., Coward, A. Madec, G., 2012. Large near-inertial oscillations of the Atlantic meridional overturning circulation. *Ocean Model*. 42(0), 50-56.

Brodeau, L., Barnier, B., Treguier, A-M., Penduff, T., Gulev, S., 2010. An ERA40-based atmospheric forcing for global ocean circulation models. *Ocean Model*. 31 (3-4), 88–104.

Chapman, P., Di Marco, S.F., Davis, R.E., Coward, A.C., 2003. Flow at intermediate depths around Madagascar based on ALACE float trajectories. *Deep Sea Res. II* 50 (12-13), 1957-1986, doi: 10.1016/S0967-0645(03)00040-7

Chassignet, E.P., Marshall, D.P., 2008. Gulf Stream Separation in Numerical Ocean Model. in *Geophysical Monograph Series, vol. 177, Ocean Modeling in an Eddying Regime*, (Eds. Hecht M.W., Hasumi, H.H.) AGU, Washington, D. C., 350pp.

Cronin, M., Watts, D.R., 1996. Eddy-mean flow interaction in the Gulf Stream at 68°W: Part I. Eddy energetics. *J. Phys. Oceanogr*., 26, 2107-2131.

Deremble, B., Hogg, A.McC., Berloff, P., Dewar, W.K., 2011. On the application of no-slip lateral boundary conditions to 'coarsely' resolved ocean models. *Ocean Model*. 39, 411-415. doi: 10.1016/j.ocemod.2011.05.002

de Ruijter, W.P.M, Ridderinkhof, H., Lutjeharms, J.R.E., Schouten, M.W., Veth, C., 2002. Observations of the flow in the Mozambique Channel. *Geophys. Res. Lett*. 29 art. no. 1502 doi: 10.1029/2001GL013714

de Ruijter, W.P.M, van Leeuwen, P.J., Lutjeharms, J.R.E., 1999. Generation and evolution of Natal Pulses: Solitary meanders in the Agulhas Current. *J. Phys. Oceanogr*. 29, 3043-3055.

Di Marco, S.F., Chapman, P. Nowlin Jr. W.D., Hacker, P., Donohue, K., Luther, M., Johnsone, G.C., Toole, J., 2002. Volume transport and property distributions of the Mozambique Channel. *Deep Sea Res. II* 49, 1481–1511.

Fransner, S.F., 2012. Effect of model settings on western boundary currents in an eddy resolving model, Master's thesis, Environmental Fluid Mechanics, Université Joseph Fourier, Grenoble, France.

Godfrey, J. S., 1989. A Sverdrup model of the depth-integrated flow for the world ocean allowing for island circulations. *Geophys. Astrophys. Fluid Dyn*. 45, 89–112.

Haidvogel, D.B., Beckmann, A., 1999. Numerical Ocean Circulation Modelling. Imperial College Press, 318 pp.

Haidvogel, D.B., McWilliams, J., Gent, P.R. 1992. Boundary current separation in a quasigeostrophic eddy-resolving ocean circulation model, *J. Phys. Oceanogr*. 22, 882-902.

Harlander, U., Ridderinkhof, H., Schouten, M.W., de Ruijter, W.P.M., 2009. Long-term observations of transport, eddies, and Rossby waves in the Mozambique Channel. *J. Geophys Res*. 114, art. no. C02003, doi: 10.1029/2008JC004846

Jaquemet, S., Le Corre, M., Quartly, G.D., 2007. Ocean control of the breeding regime of the sooty terns in the South-West Indian Ocean. *Deep Sea Res*. 54 (1), 130-142. doi: 10.1016/j.dsr.2006.10.003

Lutjeharms, J.R.E., van Ballegooyen R.C., 1988. Anomalous upstream retroflection in the Agulhas Current, Science, 240, 1770-1772.

Lutjeharms, J.R.E., Biastoch, A., van der Werf, P.M., Ridderinkhof, H., de Ruijter, W.P.M., 2012. On the discontinuous nature of the Mozambique Current. *S. Afr. J. Sci*. 108 art. no. 428, (5 pp.) doi: 10.4102/sajs.v108i1/2.428

Madec, G., and the NEMO team, 2008. NEMO ocean engine. Note du pôle de modélisation, Institut Pierre-Simon Laplace (IPSL), France, No 27, ISSN No 1288-1619.

Mariano, A.J., Chin, T.M., Özgökmen, T.M., 2003. Stochastic boundary conditions for coastal flow modeling. *Geophys. Res. Lett*. 30 (9), art. no. 1457, doi: 1029/2003GL016972

Matano, R.P., Beier, E.J., Strub, P.T., 2008. The seasonal variability of the circulation in the South Indian Ocean: Model and observations. *J. Mar. Sys*. 74, 315-328, doi: 10.1016/j.jmarsys.2008.01.007

Merryfield, W.J., Scott, R.B., 2007. Bathymetric influence on mean currents in two high-resolution near-global ocean models, *Ocean Model*. 16, 76-94, doi: 10.1016/j.ocemod.2006.07.005

Penduff, T., Le Sommer, J., Barnier, B., Treguier, A.-M., Molines, J.-M., Madec, G., 2007. Influence of numerical schemes on current-topography interactions in 1/4˚ global ocean simulations *Ocean Sci*. 3, 509–524.

Penduff, T., Juza, M., Brodeau, L., Smith, G.C., Barnier, B., Molines, J.-M., Treguier, A.-M., Madec, G., 2010. Impact of global ocean model resolution on sea-level variability with emphasis on interannual time scales. *Ocean Sci*. 6, 269–284.

Penven, P., Lutjeharms, J.R.E., Florenchie, P., 2006. Madagascar: A pacemaker for the Agulhas Current system? *Geophys. Res. Lett*. 33, art. no. L17609, doi: 10.1029/2006GL026854

Quartly, G.D., Buck, J.J.H., Srokosz, M.A., 2005. Eddy variability east of Madagascar. *Phil. Trans. Roy. Soc. Lond. A*, 363, 77-79, doi: 10.1098/rsta.2004.1479

Quartly, G.D., Buck, J.J.H., Srokosz, M.A., Coward, A.C., 2006. Eddies around Madagascar — the retroflection re-considered. *J. Mar. Sys*. 63 (3-4) 115-129. doi: 10.1016/j.jmarsys.2006.06.001

Quartly G.D., Srokosz, M.A., 2004. Eddies in the southern Mozambique Channel, *Deep Sea Res.* II, 51 (1-3), 69-83.

Saetre, R., Jorge da Silva, A., 1984. The circulation of the Mozambique channel. *Deep Sea Res*. 31 (5), 485-508.

Speich, S., Madec, G., Crépon, M., 1996, A strait outflow circulation process study: The case of the Alboran Sea. *J. Phys. Oceanogr*. 26, 320–340. doi: 10.1175/1520-0485(1996)026 <0320:ASOCPS>2.0.CO;2

Srokosz, M.A., 2003. Rapid climate change: scientific challenges and the new NERC programme. *Phil. Trans. Roy. Soc. Lond. A*, 361, 2061-2078, doi: 10.1098/rsta.2003.1243

Schouten, M.W., de Ruijter, W.P.M , van Leeuwen, P.J., Ridderinkhof, H., 2003. Eddies and variability in the Mozambique Channel. *Deep Sea Res. II,* 50 (12-13), 1987-2003. doi: 10.1016/S0967-0645(03)00042-0

van der Werf, P.M., van Leeuwen, P.J., Ridderinkhof, H., de Ruijter, W.P.M., 2010. Comparison between observations and models of the Mozambique Channel transport: Seasonal cycle and eddy frequencies. *J. Geophys. Res*., 115, art. no. C02002. doi:10.1029/2009JC005633

Verron, J., Blayo, E., 1996. The no-slip condition and separation of western boundary currents. *J. Phys. Oceanogr*. 26, 1938-1951.

Webb, D.J., de Cuevas, B.A., Coward, A.C., 1998. The first main run of the OCCAM global ocean model. *Southampton Oceanography Centre Internal Document*, No. 34, 43pp. Southampton, UK.

Zubkov, M.V., Quartly, G.D., 2003. Ultraplankton distribution in surface waters of the Mozambique Channel — flow cytometry and satellite imagery. *Aquat. Microb. Ecol.*. 33 (2), 155-161.

Table 1 : Model transports through Mozambique Channel

NEMO version	Mean (Sv)	Seasonal change (Sv)
1˚	24.9	5.1
$^1/_4$˚	26.3	5.0
$^1/_{12}$˚	24.9	7.1
$^1/_4$˚ no-slip	17.3	5.4

Mean transport is to the south, with fitted sinusoid for all runs peaking in September/October, with the amplitude of the sinusoid given in the 3rd column.

Figures

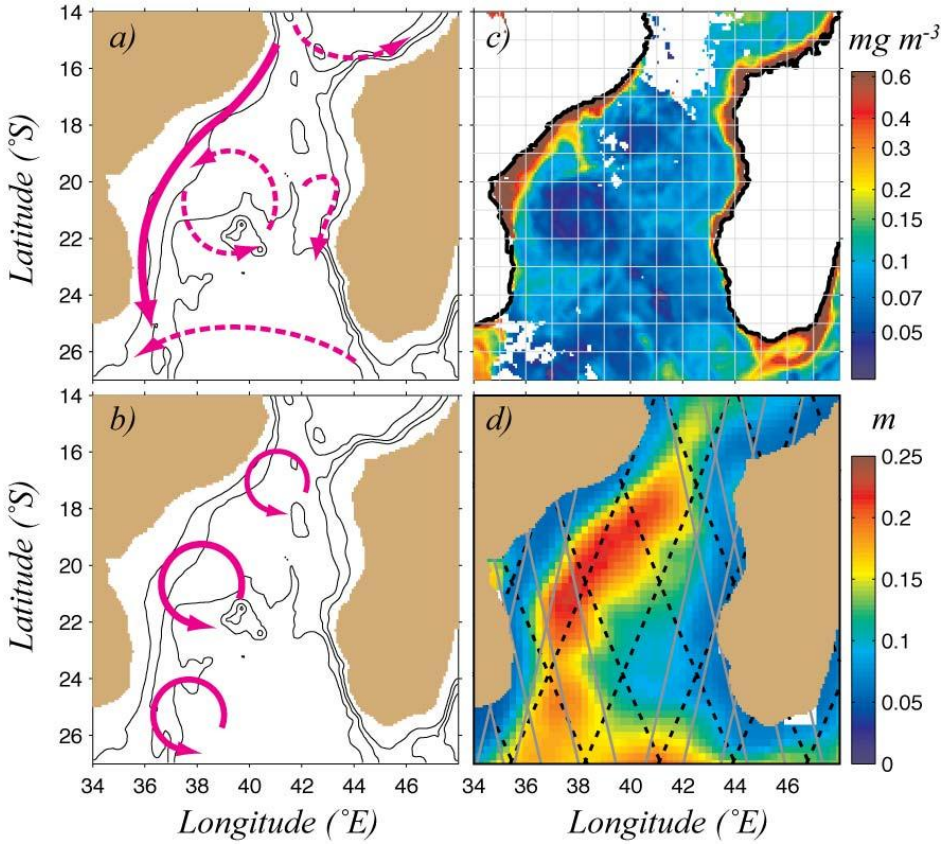

Figure 1: Flow regimes in the Mozambique Channel a) Schematic of original understanding of strong western boundary current (solid line) or gyral circulation (dashed lines) advocated by Saetre and Jorge da Silva (1984). b) Schematic of flow from recent hydrographic observations of anticyclonic eddies heading southward along western edge of channel. c) Chlorophyll concentration (MODIS composite: 5th-12th March 2012).revealing large circular low-chlorophyll structures. d) R.m.s. variability of sea surface height from satellite altimetry (Black dashed and grey full lines indicate sampling by Topex/Jason and ERS/Envisat respectively in a typical 10-day period.)

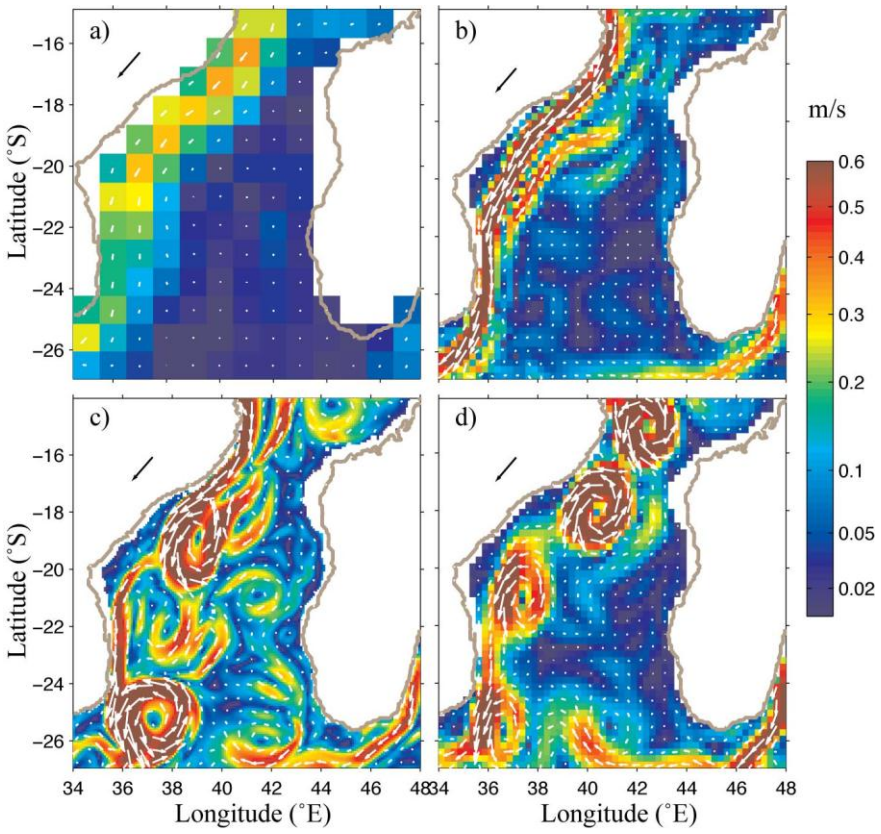

Fig. 2: Example 5-day snapshots at 26.6 m from different NEMO models for 13th-17th Sept. 1998. a) 1˚, b) $^1/_4$˚, c) $^1/_{12}$˚ free-slip runs, d) $^1/_4$˚ run with no-slip boundary conditions applied. Non-linear colour scale shows speed; reference arrow (on land) is 0.25 m s^{-1}. (Note for b)-d) arrows are only plotted every 0.5˚.)

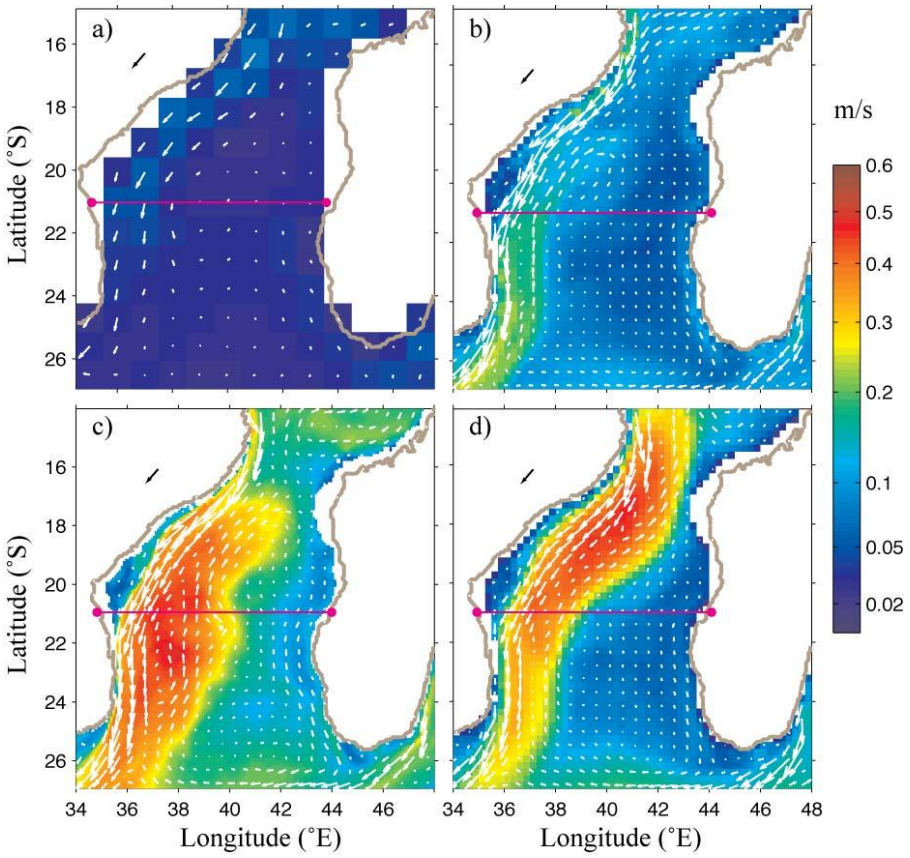

Fig. 3: Mean and variability of flow at 26.6 m in the different NEMO models a) 1˚, b) $^1/_4$˚, c) $^1/_{12}$˚ free-slip runs d) $^1/_4$˚ run with no-slip boundary conditions applied. Arrows show mean over 1997-2001; non-linear colour scale shows r.m.s. variability; reference arrow is 0.25 m s^{-1}. Pink lines show section at 21˚S discussed later. (Note for b)-d) arrows are only plotted every 0.5˚.)

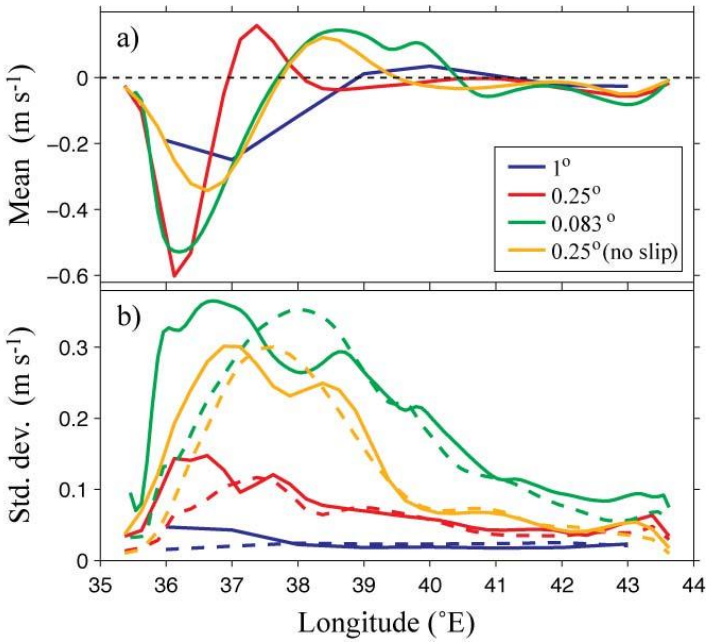

Fig. 4: Mean and variability of flow at 26.6 m for a zonal section near 21˚S. a) Mean meridional current, b) Standard deviation of meridional current (full line) and zonal current (dashed line).

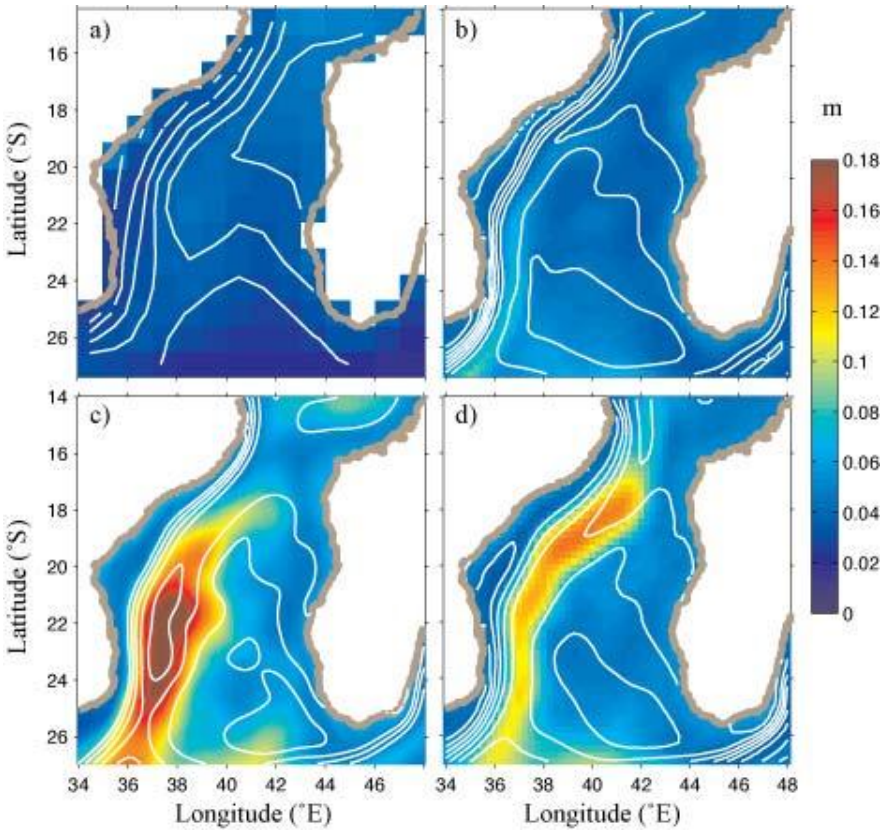

Fig. 5: Mean and variability of dynamic height in the different NEMO models a) 1˚, b) $^1/_4$˚, c) $^1/_{12}$˚ free-slip runs d) $^1/_4$˚ run with no-slip boundary conditions applied. The colour scale shows r.m.s. variability during 1997-2001; white lines show the mean dynamic height, with contours every 0.05 m.

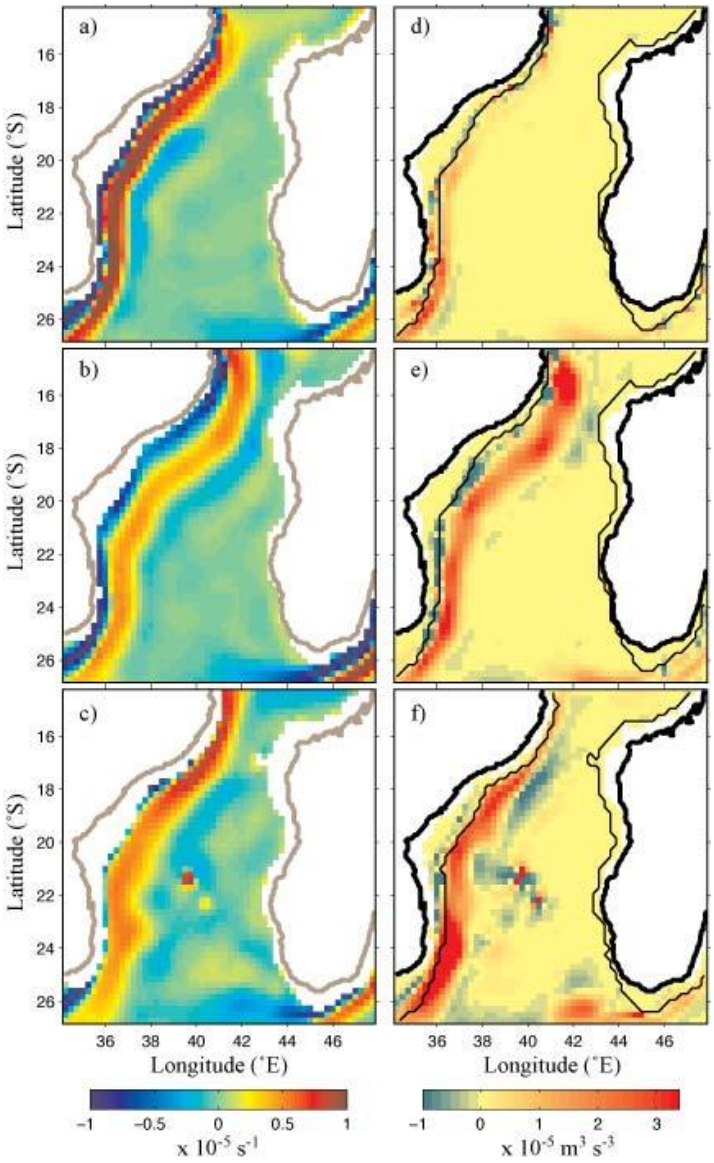

Fig. 6: Vorticity averaged over 25-200m depth and the period 1997-2001. a) $^1/_4^\circ$ free-slip, b) $^1/_4^\circ$ no-slip, c) $^1/_{12}^\circ$ free-slip. BTI averaged over 1997-2001. d) $^1/_4^\circ$ free-slip, e) $^1/_4^\circ$ no-slip, f) $^1/_{12}^\circ$ free-slip runs. The added black contours show the 1100m isobath.

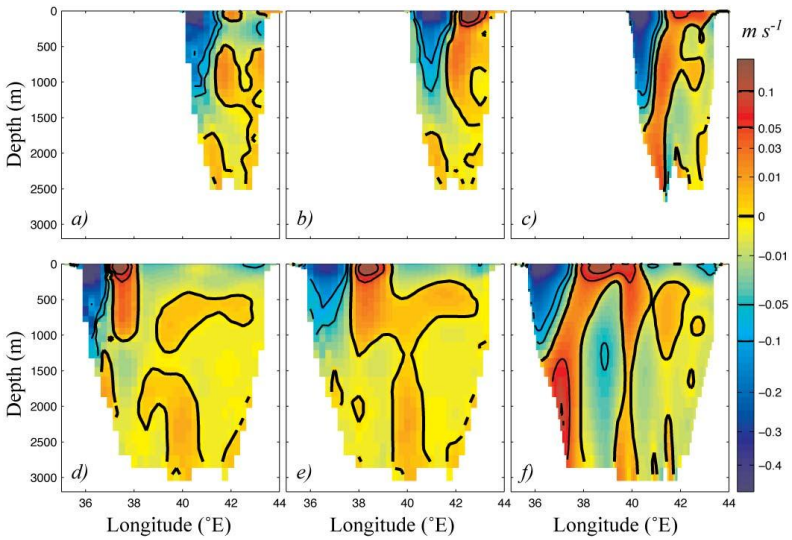

Fig. 7: Mean meridional velocity across Mozambique Channel at 16.5˚S (upper row) and 21˚S (lower row). a),d) are from NEMO $^1/_4^\circ$ free-slip run; b),e) are from $^1/_4^\circ$ no-slip run; c),f) are from $^1/_{12}^\circ$ free-slip run. Non-linear colour scale is used to reveal the details near zero, with the 0, ±0.05 and ±0.10 m s^{-1} isotachs highlighted.

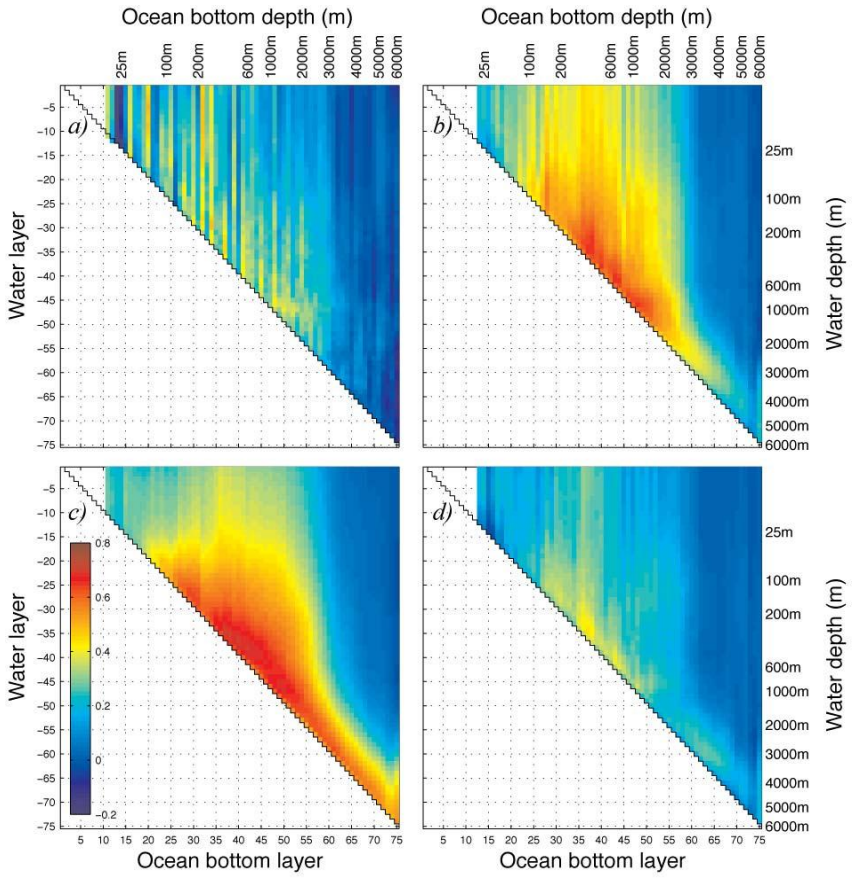

Fig. 8: Topostrophy (see Penduff et al., 2007) showing correlation of mean velocity vector with bathymetric contours. a) 1˚, b) $^1/_4$˚, c) $^1/_{12}$˚ resolution runs with free-slip, d) $^1/_4$˚ run with no-slip conditions.

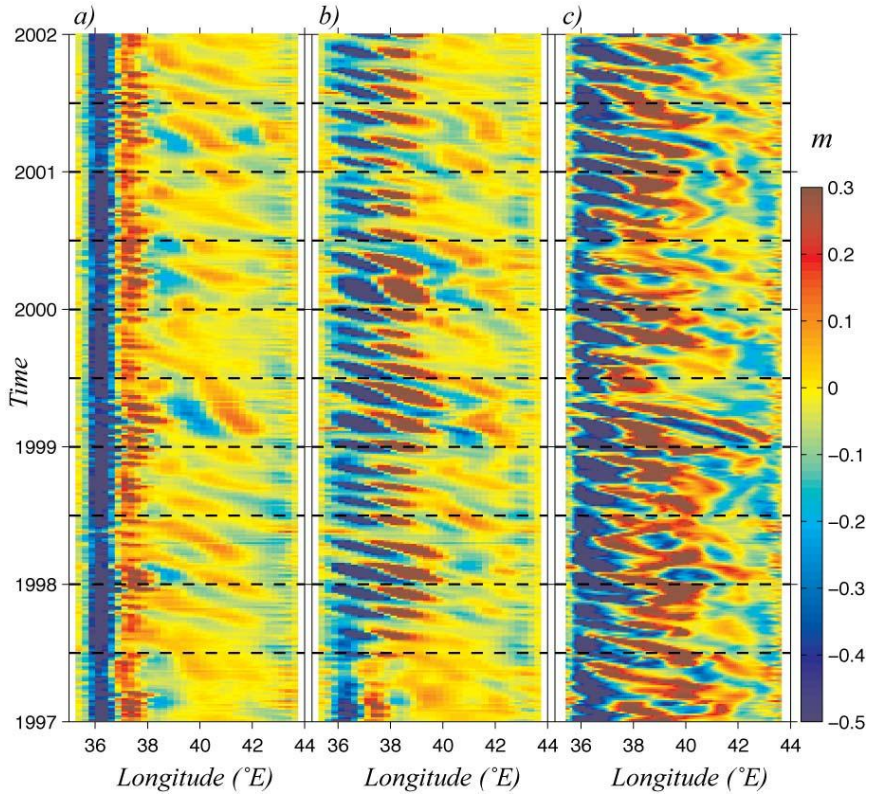

Fig. 9: Hovmöller diagrams of meridional current at 26.6 m for a zonal section near 21˚S. a) Standard $^1/_4$˚ run with free-slip boundary conditions, b) $^1/_4$˚ no-slip run, c) $^1/_{12}$˚ free-slip run.

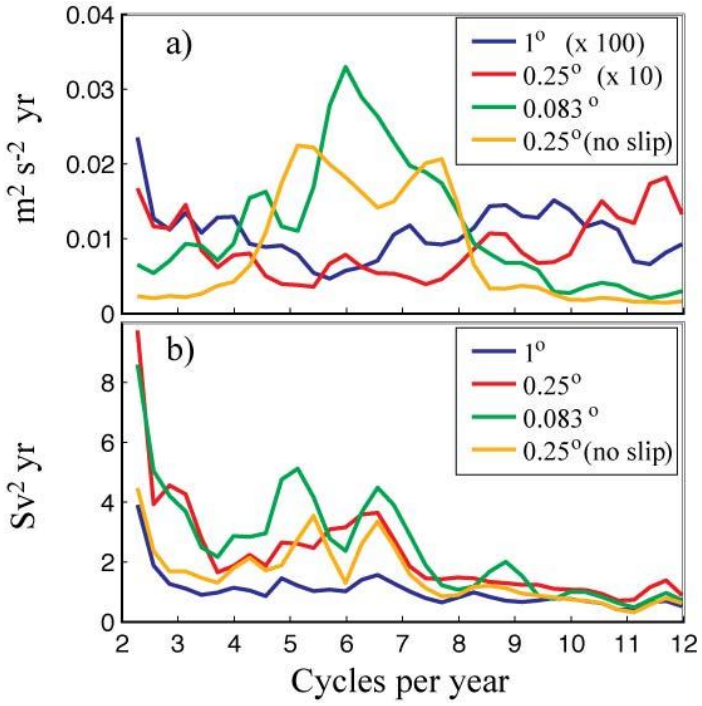

Fig. 10: High-frequency variability in the flow at 21˚S. a) Meridional current at 26.6 m at location of peak variability (see Fig. 4b). b) Full depth-integrated transport across section. (Note multipliers are applied to red and blue lines in top plot only.)

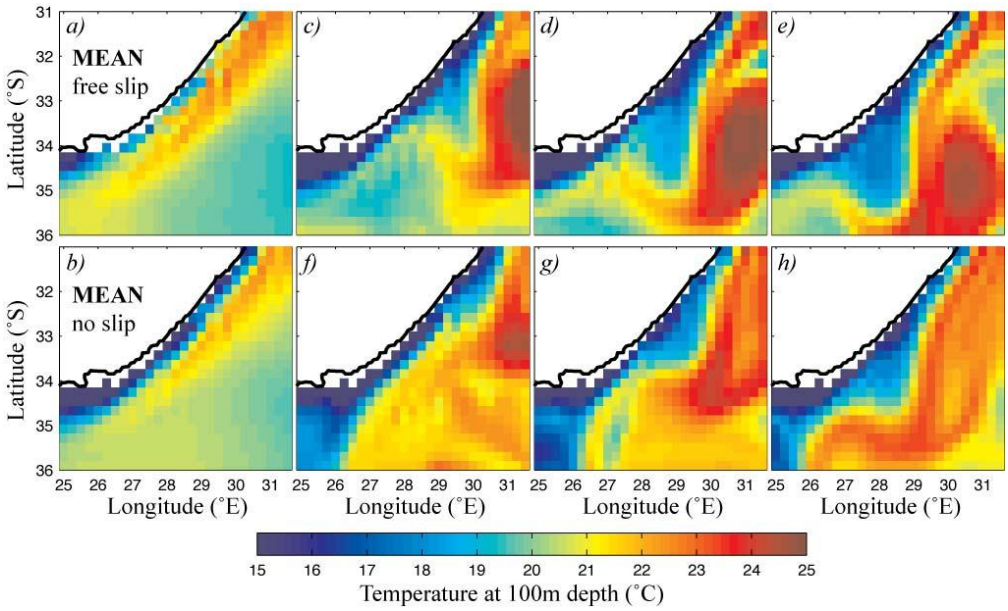

Fig. 11: Offshore instability of the Agulhas Current in $^{1}/_{4}^{\circ}$ resolution models. a) Mean of 1997-2007 output for free-slip run. b) Same for no-slip. c-e) Three snapshots 10 days apart from no-slip run in April-May 1998 showing a Natal Pulse f-h) Similar (no-slip again) for May-June 2003.